

# Continuous-time parametrization of neural quantum states for quantum dynamics

Dingzu Wang,<sup>1</sup> Wenxuan Zhang,<sup>1</sup> Xiansong Xu,<sup>2,3</sup> and Dario Poletti<sup>3,4,1,5</sup>

<sup>1</sup>*Centre for Quantum Technologies, National University of Singapore 117543, Singapore*

<sup>2</sup>*College of Physics and Electronic Engineering, and Center for Computational Sciences, Sichuan Normal University, Chengdu 610068, China*

<sup>3</sup>*Science, Mathematics and Technology Cluster, Singapore University of Technology and Design, 8 Somapah Road, 487372 Singapore*

<sup>4</sup>*EPD Pillar, Singapore University of Technology and Design, 8 Somapah Road, 487372 Singapore*

<sup>5</sup>*MajuLab, CNRS-UNS-NUS-NTU International Joint Research Unit, UMI 3654, Singapore*

(Dated: July 14, 2025)

Neural quantum states are a promising framework for simulating many-body quantum dynamics, as they can represent states with volume-law entanglement. As time evolves, the neural network parameters are typically optimized at discrete time steps to approximate the wave function at each point in time. Given the differentiability of the wave function stemming from the Schrödinger equation, here we impose a time-continuous and differentiable parameterization of the neural network by expressing its parameters as linear combinations of temporal basis functions with trainable, time-independent coefficients. We test this ansatz, referred to as the smooth neural quantum state (*s*-NQS) with a loss function defined over an extended time interval, under a sudden quench of a non-integrable many-body quantum spin chain. We demonstrate accurate time evolution using simply a restricted Boltzmann machine as the instantaneous neural network architecture. Furthermore, we demonstrate that the parameterization is efficient in the number of parameters and the smooth neural quantum state allows us to initialize and evaluate the wave function at times not included in the training set, both within and beyond the training interval.

## I. INTRODUCTION

The study of the dynamics of quantum many-body systems plays a central role in understanding fundamental aspects of quantum statistical mechanics [1]. Driven by recent experimental and theoretical progress, research in this area has rapidly advanced, enabling unprecedented access to coherent real-time evolution and revealing a range of nonequilibrium phenomena, including prethermalization [2–6], many-body localization [7, 8], dynamical quantum phase transitions [9, 10], many-body scars [11], and slow relaxation regimes [12]. Despite these advances, simulating such dynamics remains a major challenge in computational quantum physics, primarily due to the exponential growth of the Hilbert space with system size, which renders exact approaches intractable. Tensor network methods provide an efficient representation for area-law entangled states in one-dimensional systems and have achieved notable success, but they struggle to accurately simulate higher-dimensional systems or states with complex entanglement [13–15].

Neural quantum states (NQS), which represent quantum wave functions using artificial neural networks, have recently emerged as a flexible variational ansatz capable of describing volume-law states, even in dimensions larger than one [16–18]. Over the past few years, NQS have been successfully applied to compute time evolution of many-body quantum systems, both for unitary [19–29] and dissipative [30–34] systems. Several approaches have been developed to evolve the networks in time, including time-dependent variational Monte Carlo (tVMC) [35], its projective extension (p-tVMC) [36], and more recently proposed global loss-based optimization schemes [27, 28].

A review of the current state of the art is provided in Ref. [37], and important technical details concerning sampling strategies and loss functions can be found in Ref. [26]. Meanwhile, Ref. [25] presents an approach to incorporating stochastic reconfiguration [38, 39] within the p-tVMC framework for time evolution. However, notwithstanding these developments, reliably capturing the dynamics of quantum many-body systems using NQS remains highly nontrivial.

In isolated quantum systems, the Schrödinger equation induces a unitary and continuous evolution of the quantum state in Hilbert space, suggesting that the dynamics is amenable to variational representations that are continuous and differentiable in time. Motivated by this insight, we propose a continuous and differentiable parametrization in time of the neural network ansatz, which we refer to as *smooth* neural quantum state (*s*-NQS) ansatz (see Fig. 1). Specifically, each time-evolving parameter  $\vartheta_j(t)$  in the *s*-NQS is defined as a linear combination of smooth temporal functions, e.g., polynomials, with time-independent variational parameters  $\{\theta_{j,q}\}$ . This parametrization allows for the network to accurately represent quantum states not only at discrete training times but also at unoptimized points within the same time interval  $\tau$  through interpolation (see Fig. 1). Moreover, by extending the temporal functions beyond the training interval, the *s*-NQS can simulate quantum states at later times. This feature provides a well-informed initialization for the subsequent interval, which can accelerate convergence and significantly enhance training stability.

For each interval, the parameters of the *s*-NQS are determined by smooth temporal functions and variational

parameters. This parameterization enables the definition of a global loss function over each time interval, which may reduce error accumulation compared to step-by-step schemes. Note that the use of global loss functions and time-dependent networks, has also been explored in recent studies [27, 28], showing promising results. However, our method employs a distinct loss formulation and a different network parameterization. We demonstrate the effectiveness of our method by simulating quantum quenches—where the system is initially prepared in the ground state of one Hamiltonian and subsequently evolved under a different one as done, for example, in studies of thermalization [40–45].

The paper is organized as follows: in Sec. II, we introduce the *smooth* neural quantum state ansatz, the *s*-NQS; in Sec. III, we describe the optimization strategy for the *s*-NQS, from the loss function to the gradient computation; in Sec. IV we show our results for the Hamiltonian quench considered, and draw our conclusions in Sec. V. More details about the method and the calculations can be found in App. A-B.

## II. THE *s*-NQS ANSATZ

In this section, we introduce the *smooth* neural quantum state ansatz. Within this approach, a wave function at time  $t$ ,  $|\psi(t)\rangle$ , is approximated by  $|\psi_{\boldsymbol{\vartheta}(t)}\rangle$  using a set of time-evolving network parameters  $\boldsymbol{\vartheta}(t) = \{\vartheta_1(t), \dots, \vartheta_j(t), \dots, \vartheta_{N_p}(t)\}$ , where each  $\vartheta_j(t)$  is defined as a linear combination of smooth temporal basis functions  $\{g_q(t)\}$  and a set of variational parameters  $\{\theta_{j,q}\}$

$$\vartheta_j(t) = \sum_{q=0}^{Q-1} g_q(t) \cdot \theta_{j,q}, \quad (1)$$

where  $Q$  is the number of temporal basis functions. This construction ensures that the temporal behavior of the network parameters is intrinsically smooth, a property that is encoded directly into the parameterization, as schematically illustrated in Fig. 1. The derivative variational parameters can be written as

$$\frac{\partial}{\partial \theta_{j,q}} = \frac{\partial}{\partial \vartheta_j} \frac{\partial \vartheta_j}{\partial \theta_{j,q}} = g_q(t) \frac{\partial}{\partial \vartheta_j}. \quad (2)$$

This allows us to compute derivatives with respect to  $\theta_{j,q}$  at a given time. In this work, we use shifted Chebyshev polynomials  $\mathcal{T}_q$  as the temporal basis functions  $g_q(t)$ ,

$$g_q(t) = \mathcal{T}_q(r(t)), \quad (3)$$

where  $\mathcal{T}_q$  denotes the  $q$ -th Chebyshev polynomial and  $r(t)$  rescales the time variable such that  $r(t) \in [-1, 1]$  (see App. A for details). The choice of temporal basis functions could influence the expressivity and stability of the *s*-NQS, and we leave a detailed investigation of this aspect for future work.

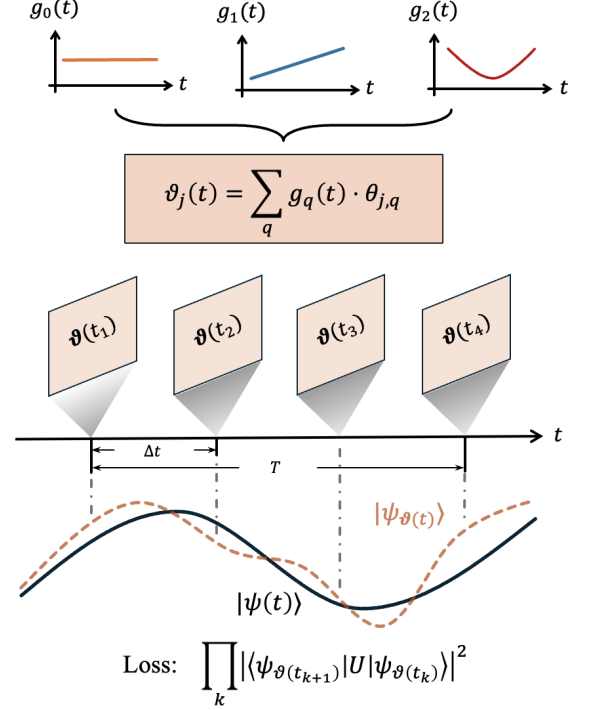


FIG. 1. Schematic illustration of the *s*-NQS approach. Top: the temporal basis functions  $\{g_q(t)\}$  are linearly combined with time-independent coefficients  $\{\theta_{j,q}\}$  to construct the network parameter  $\vartheta_j(t)$ . Middle: these parameters determine the variational wave function  $|\psi_{\boldsymbol{\vartheta}(t)}\rangle$  (brown dashed line), within a time interval  $\tau$  composed of smaller steps  $\Delta t$ . Bottom: the parameters are optimized by minimizing a global loss function that enforces consistency with the exact evolution state  $|\psi(t)\rangle$  (black solid line) over the entire interval.

To specify the wave function representation within the *s*-NQS framework, we adopt the restricted Boltzmann machine (RBM) architecture, which was introduced in Ref. [35] as the first neural-network-based ansatz for quantum states. The RBM is a shallow, fully connected neural network and allows for an explicit and analytic expression of the wave function. For a quantum spin system with  $L$  sites, the RBM maps each spin configuration  $\mathbf{x} = (x_1, \dots, x_L)$ , where  $x_i \in \{-1, +1\}$ , to an unnormalized wave function  $\psi(\mathbf{x}) \in \mathbb{C}$ , given by  $\psi_{\boldsymbol{\vartheta}(t)}(\mathbf{x}) = \langle \mathbf{x} | \psi_{\boldsymbol{\vartheta}(t)} \rangle$ , expressed as

$$\psi_{\boldsymbol{\vartheta}(t)}(\mathbf{x}) = \exp \left( \sum_{i=1}^L a_i(t) x_i \right) \times \prod_{j=1}^M 2 \cosh \left( b_j(t) + \sum_{i=1}^L W_{i,j}(t) x_i \right), \quad (4)$$

where  $\boldsymbol{\vartheta}(t) = \{\mathbf{a}(t), \mathbf{b}(t), \mathbf{W}(t)\}$  represents a set of complex-valued parameters of the RBM:  $a_i(t)$  and  $b_j(t)$  are visible and hidden biases, respectively, and  $W_{i,j}(t)$  are elements of the weight matrix. The visible layer takes the spin configuration as input, while the hid-

den layer captures nontrivial correlations via the non-linear activation. We set the number of hidden units to  $M = \alpha L$ , where  $\alpha \in \mathbb{Z}^+$  determines the number of hidden units and affects the expressive capacity of the network. All network parameters are time-dependent following the smooth parametrization defined in Eq. (1) and collectively grouped into the vector  $\boldsymbol{\theta}(t)$ . Owing to its analytic structure, the RBM allows for closed-form evaluation of the wave function and logarithmic derivatives with respect to network parameters.

### III. VARIATIONAL OPTIMIZATION SCHEME

We consider the unitary time evolution of a quantum state governed by the Schrödinger equation (working in units such that  $\hbar = 1$ ),

$$\frac{d}{dt}|\psi(t)\rangle = -i\hat{H}|\psi(t)\rangle. \quad (5)$$

The solution is given by the application of the time evolution operator  $\hat{U}(t)$  to the initial state  $|\psi(0)\rangle$ ,

$$|\psi(t)\rangle = \hat{U}(t)|\psi(0)\rangle, \quad (6)$$

where  $\hat{U}(t) = \exp(-i\hat{H}t)$ .

In numerical simulations, we discretize time using a small *time step*  $\Delta t$ , which allows for an approximate implementation of the evolution operator. This is particularly relevant for large systems, where exact evaluation of  $\hat{U}(t)$  is typically intractable and approximate methods are required. Further details regarding the approximation of  $\hat{U}$  will be presented in Sec. III C and App. B. To manage the evolution over longer time ranges, we introduce two additional temporal scales that structure our optimization procedure. The first is the *time interval*  $\tau$ , which consists of several consecutive time steps and defines the domain over which the variational parameters of the *s*-NQS ansatz are optimized globally. The second is the *time window*  $T$ , which comprises multiple such intervals and sets the support of the temporal basis functions  $g_q(t)$ . In the following, we introduce the loss function used to train the *s*-NQS within each interval, describe how its gradients are evaluated, present the approximation of the evolution operator, and explain how the long-time evolution is assembled across successive time windows.

#### A. Global loss function over time intervals

To determine the variational parameters of the *s*-NQS within each time interval, we define a global loss function that quantifies the fidelity between the network state and its time-evolved counterpart. The loss is defined as

$$\mathcal{C}(\{\theta_{j,q}\}) = \prod_{k=0}^K \mathcal{C}_k(\{\theta_{j,q}\}), \quad (7)$$

where  $K$  is the number of time steps  $\Delta t$  within the interval  $\tau$ , and  $\mathcal{C}_k$  quantifies the fidelity at each step. For  $k \neq 0$ , we define

$$\mathcal{C}_k(\{\theta_{j,q}\}) = \frac{\langle \psi_{\boldsymbol{\theta}(t'')} | \hat{U} | \psi_{\boldsymbol{\theta}(t')} \rangle \langle \psi_{\boldsymbol{\theta}(t')} | \hat{U}^\dagger | \psi_{\boldsymbol{\theta}(t'')} \rangle}{\langle \psi_{\boldsymbol{\theta}(t'')} | \psi_{\boldsymbol{\theta}(t'')} \rangle \langle \psi_{\boldsymbol{\theta}(t')} | \psi_{\boldsymbol{\theta}(t')} \rangle}, \quad (8)$$

with  $t' = t_0 + (k-1)\Delta t$  and  $t'' = t_0 + k\Delta t$  and, for brevity, we denote  $\hat{U}(\Delta t)$  simply as  $\hat{U}$ . Each  $\mathcal{C}_k$  corresponds to the normalized overlap between the variational states before and after time evolution. This loss function correctly reflects Hilbert-space distance between quantum states and is structurally similar to the one used in the projected time-dependent variational Monte Carlo (p-tVMC) approach [21, 25, 26]. At the initial time step  $k = 0$ , we include the initial state  $|\psi(t_0)\rangle$  in the loss function as

$$\mathcal{C}_0(\{\theta_{j,q}\}) = \frac{\langle \psi_{\boldsymbol{\theta}(t_0)} | \psi(t_0) \rangle \langle \psi(t_0) | \psi_{\boldsymbol{\theta}(t_0)} \rangle}{\langle \psi_{\boldsymbol{\theta}(t_0)} | \psi_{\boldsymbol{\theta}(t_0)} \rangle \langle \psi(t_0) | \psi(t_0) \rangle}, \quad (9)$$

where  $|\psi(t_0)\rangle$  corresponds to the known representation of wave function at the beginning of the interval. We then maximize the loss function  $\mathcal{C}$  to optimally determine the *s*-NQS representation of the time-evolved states across the interval.

The structure of the *s*-NQS ansatz plays a key role in the optimization process. Specifically, the smooth temporal functions  $g_q(t)$  naturally capture the continuity within and across intervals. In practice, each network parameter at time  $t_c$  within the current interval can be initialized from the previous interval

$$\vartheta_j(t_c) = \sum_q g_q(t_c) \cdot \theta_{j,q}^{[t_0-\tau, t_0]}, \quad (10)$$

where we used the notation  $\theta_{j,q}^{[t_0-\tau, t_0]}$  to specify that these variational parameters have been optimized in the time interval  $[t_0-\tau, t_0]$ , while  $t_c$  is in the following time interval  $t_c \in [t_0, t_0 + \tau]$ . Owing to the smooth parametrization, the resulting network states—evaluated using parameters from the previous interval—are typically already close to the optimal representation in the current one, as we will show later. As a result, it accelerates convergence and improves the overall stability of the training process.

Another key point is the definition of the  $\mathcal{C}_0$  term in the global loss function [Eq. (7)]. Here,  $\mathcal{C}_0$  does not involve the time-evolution operator  $\hat{U}$  and instead directly measures the overlap between the variational state and the known initial state. This alignment between initialization and loss structure further enhances the stability and efficiency of the optimization process.

#### B. Gradient evaluation

The variational parameters  $\theta_{j,q}$  are optimized over each time interval  $\tau$  using gradient descent

$$\theta_{j,q} \leftarrow \theta_{j,q} - \eta \frac{\partial \mathcal{C}}{\partial \theta_{j,q}}, \quad (11)$$

where  $\eta$  is the learning rate. To evaluate the gradient of the global loss function  $\mathcal{C}$  under the smooth parameterization of the  $s$ -NQS, we use the chain rule to obtain

$$\begin{aligned} \frac{\partial \mathcal{C}}{\partial \theta_{j,q}} &= \sum_{k=0}^K \left( \prod_{k' \neq k} c_{k'} \right) \frac{\partial \mathcal{C}_k}{\partial \theta_{j,q}} \\ &= \sum_{k=0}^K \left( \prod_{k' \neq k} c_{k'} \right) \frac{\partial \mathcal{C}_k}{\partial \vartheta_j} \cdot g_q(t_k), \end{aligned} \quad (12)$$

where  $t_k = t_0 + k\Delta t$ . This expression follows from the smooth parameterization in Eq. (1), where each  $\theta_{j,q}$  contributes to the full time-dependent parameter  $\vartheta_j(t)$  through the smooth temporal function  $g_q(t)$ .

The value of each  $\mathcal{C}_k$  for  $k \neq 0$  is given by

$$\mathcal{C}_k = \left[ \sum_{\mathbf{x}} P_{t''}(\mathbf{x}) \mathcal{C}_{\text{loc}}^{t''}(\mathbf{x}) \right] \left[ \sum_{\mathbf{y}} P_{t'}(\mathbf{y}) \mathcal{C}_{\text{loc}}^{t'}(\mathbf{y}) \right], \quad (13)$$

where the local estimators are defined as

$$\mathcal{C}_{\text{loc}}^{t''}(\mathbf{x}) = \sum_{\mathbf{x}'} \frac{\psi_{\vartheta(t'')}(\mathbf{x}')}{\psi_{\vartheta(t'')}(\mathbf{x})} \langle \mathbf{x} | \hat{U} | \mathbf{x}' \rangle, \quad (14)$$

$$\mathcal{C}_{\text{loc}}^{t'}(\mathbf{y}) = \sum_{\mathbf{y}'} \frac{\psi_{\vartheta(t')}(\mathbf{y}')}{\psi_{\vartheta(t')}(\mathbf{y})} \langle \mathbf{y} | \hat{U}^\dagger | \mathbf{y}' \rangle. \quad (15)$$

For  $k = 0$ , the time-evolution operators reduce to the identity, resulting in Kronecker deltas  $\delta(\mathbf{x}, \mathbf{x}')$  and  $\delta(\mathbf{y}, \mathbf{y}')$  in the local estimators. The probabilities are given by

$$P_{t''}(\mathbf{x}) = \frac{|\psi_{\vartheta(t'')}(\mathbf{x})|^2}{\langle \psi_{\vartheta(t'')} | \psi_{\vartheta(t'')} \rangle}, \quad P_{t'}(\mathbf{y}) = \frac{|\psi_{\vartheta(t')}(\mathbf{y})|^2}{\langle \psi_{\vartheta(t')} | \psi_{\vartheta(t')} \rangle}. \quad (16)$$

The Hilbert space dimension grows exponentially with system size. Therefore, we employ Monte Carlo (MC) sampling to evaluate both the local estimators and the associated probabilities for large systems. The gradients  $\partial \mathcal{C}_k / \partial \vartheta_j$  can be computed either analytically or using automatic differentiation. In this work, we employ the AdamW optimizer [46] to update  $\theta_{j,q}$ .

### C. Approximate evaluation of the evolution operator

In large many-body systems, the exact application of the evolution operator  $\hat{U} = e^{-i\hat{H}\Delta t}$  is computationally intractable, as  $\hat{U}$  is a dense operator whose action on a basis state involves exponentially many nonzero terms. To overcome this challenge, several approximation strategies have been proposed, including Trotter-Suzuki decomposition that splits the evolution into local terms Ref. [47, 48], Taylor expansions around small time steps, and multiplicative schemes such as those introduced in Ref.

[26]. Here, we adopt a second-order Taylor expansion of the form

$$\hat{U}(\Delta t) \approx \hat{\mathbb{I}} - i\Delta t \hat{H} - \frac{1}{2}(\Delta t \hat{H})^2, \quad (17)$$

where  $\hat{\mathbb{I}}$  denotes the identity operator and  $\Delta t$  is assumed to be small enough such that higher-order terms can be neglected. This approximation yields a simple analytic form for  $\hat{U}$  and enables efficient Monte Carlo sampling in high-dimensional Hilbert spaces. When higher accuracy is desired, higher-order Taylor expansions remain fully compatible with our framework and can be incorporated, although multiplicative schemes would be preferred [26]. More details can be found in App. B.

### D. Continuity across time windows

In this context, the smooth temporal basis functions  $g_q(t)$  are defined over a rescaled time domain  $r(t) \in [-1, 1]$ , which corresponds to a finite segment of physical time referred to as a time window  $T$ . As a consequence, the smooth parameterization of the  $s$ -NQS is inherently confined to this window. To extend the simulation beyond a single time window while preserving temporal flexibility, we assemble the full time evolution by sequentially joining multiple windows.

A key advantage of the  $s$ -NQS framework is that it provides not only the values of the network parameters at any given time, but also their time derivatives. By evaluating those values at the window boundary, the  $s$ -NQS enables smooth continuation into the next time window. For example, in the first time window from  $t = 0$  to  $t = T$ , the network parameters are given by

$$\vartheta_j(t) = \sum_{q=0}^{Q-1} \mathcal{T}_q(r_1(t)) \cdot \theta_{j,q}^{[0, T]}, \quad (18)$$

where  $r_1(t)$  denotes the rescaled time in the first window and  $\theta_{j,q}^{[0, T]}$  means the variational parameters are optimized in the time window  $[0, T]$ . In the subsequent window, we define a new parameterization

$$\vartheta_j(t) = \sum_{q=0}^{Q-1} \mathcal{T}_q(r_2(t)) \cdot \theta_{j,q}^{[T, 2T]} \quad (19)$$

At the interface between two time windows, we enforce continuity of all time derivatives of the network parameters. This leads to the matching condition

$$\begin{aligned} \frac{d^n}{dt^n} \left[ \sum_q \theta_{j,q}^{[0, T]} \cdot \mathcal{T}_q(r_1(t)) \right]_{r_1(t)=1} \\ = \frac{d^n}{dt^n} \left[ \sum_{q'} \theta_{j,q'}^{[T, 2T]} \cdot \mathcal{T}_{q'}(r_2(t)) \right]_{r_2(t)=-1} \end{aligned} \quad (20)$$

This matching condition ensures the continuity of the  $n$ -th time derivatives of the network parameters across time windows. More details can be found in App. A.

#### IV. SIMULATION OF A HAMILTONIAN QUENCH

To demonstrate the effectiveness of the  $s$ -NQS approach in simulating quantum many-body dynamics, we consider the tilted Ising model (TIM) with open boundary conditions. The Hamiltonian for a system with  $L$  spins is given by

$$\hat{H} = J \sum_{i=1}^{L-1} \hat{\sigma}_i^z \hat{\sigma}_{i+1}^z - \sum_{i=1}^L (h_x \hat{\sigma}_i^x + h_z \hat{\sigma}_i^z), \quad (21)$$

where  $J$  is the nearest-neighbor coupling constant,  $h_x$  and  $h_z$  denote external magnetic fields along the  $x$ - and  $z$ -directions respectively, and  $\hat{\sigma}_i^a$  (with  $a = x, y, z$ ) are Pauli operators acting on site  $i$ . This system is known to be interacting and nonintegrable unless one of the fields  $h_x$  or  $h_z$  is zero, and it has been extensively used to study eigenstate thermalization hypothesis [49, 50] and many-body quantum chaos [51]. When  $J$  dominates over  $h_x$ , the ground state is either ferromagnetic or antiferromagnetic. Conversely, when  $h_x$  dominates, the ground state is paramagnetic. In the case of  $h_z = 0$ , the model reduces to the integrable transverse field Ising model which, in 1D, exhibits a quantum phase transition at the critical point  $J = h_x$ .

In our simulations, we initialize the system in paramagnetic product state of the form

$$|\psi(0)\rangle = \bigotimes_{i=1}^L \frac{1}{\sqrt{2}} (|0\rangle_i + |1\rangle_i), \quad (22)$$

where  $|0\rangle_i$  and  $|1\rangle_i$  denote the eigenstates of  $\sigma_i^z$  on site  $i$ . This state corresponds to the ground state of the Hamiltonian in the limit  $h_x \gg J$  and  $h_z$ , where transverse field dominates and the system is deep in the paramagnetic phase. We then quench the Hamiltonian parameters into a regime in which the ground state exhibits antiferromagnetic correlations.

##### A. Benchmarking $s$ -NQS on a fully computable small system

To evaluate the intrinsic performance of the  $s$ -NQS ansatz, we first focus on a small spin system where all quantities can be computed exactly without approximations. Specifically, we consider a spin chain of length  $L = 10$ , for which all observables and gradients can be evaluated exactly by summing over the full basis of  $2^{10} = 1024$  configurations, and the evolution operator  $\hat{U} = \exp(-i\hat{H}\Delta t)$  can be directly exponentiated. We choose Hamiltonian parameters  $h_x = h_z = 0.3J$ , and use

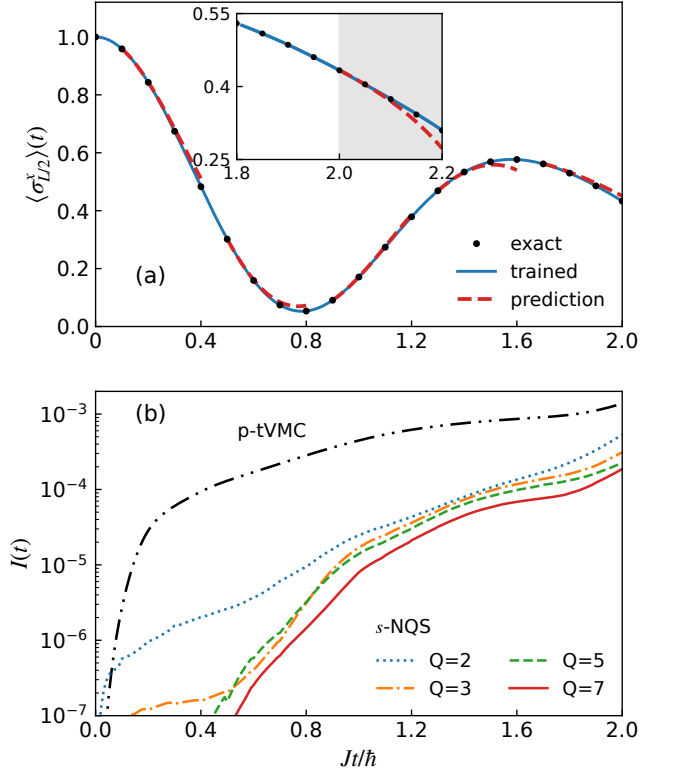


FIG. 2. Quench dynamics of 1D tilted Ising model with open boundary conditions. (a) Time evolution of the transverse magnetization of the middle site  $\langle \sigma_{L/2}^x \rangle(t)$ ; (b) Time evolution of the infidelity between numerical solutions and the exact results. We compare the performance of p-tVMC with  $s$ -NQS for different values of the temporal expressivity parameter  $Q$ . Parameters are  $\alpha = 5$ ,  $Jdt/\hbar = 0.01$ ,  $L = 10$ ,  $h_x = h_z = 0.3J$  and  $J\tau/\hbar = 0.1$ .

a time step  $J\Delta t = 0.01$  with time intervals  $J\tau = 0.1$ . The evolution is performed up to  $Jt = 2.2$ , while the time window is set to  $JT = 2.0$ , which implies that we need to connect two different windows.

Fig. 2(a) shows the time evolution of the transverse magnetization at the center of the chain,  $\langle \sigma_{L/2}^x \rangle(t)$ . Exact results are represented by black dots, while the solid blue line denotes the  $s$ -NQS simulation using the temporal basis size  $Q = 3$  and a RBM with  $\alpha = 5$ . The excellent agreement shows the accuracy of the ansatz when trained within a time interval.

A key strength of the  $s$ -NQS lies in its smooth parameterization, which naturally provides high-quality initializations for adjacent, yet-to-be-trained intervals. This is illustrated in Fig. 2(a) by the red dashed lines, which show the network prediction in multiple untrained intervals using only the parameters optimized in the preceding interval. For instance, the first dashed line (from  $t = \tau$  to  $t = 4\tau$ ) is obtained directly from training over the interval  $t \in [0, \tau]$ , without further optimization. Similarly, training from  $t = 4\tau$  to  $5\tau$  enables prediction from  $5\tau$  to  $8\tau$ . These results demonstrate that the smooth structure



already provides near-optimal initialization, enabling accurate predictions even before additional training is performed.

The inset of Fig. 2(a) highlights the performance of the  $s$ -NQS when bridging across adjacent time windows. The first time window ends at  $t = T = 2/J$ , after which the parameters for the subsequent window are initialized using the continuity conditions defined in Eq. (20). Without any additional training in the second window, the resulting red dashed line accurately reproduces the observable's evolution up to  $t \approx 2.1/J$ , demonstrating the strength of the smooth initialization. Upon further optimization within the new window, the final trained trajectory (solid blue line) aligns precisely with the exact result, as indicated by the black dots.

In Fig. 2(b), we show the infidelity of the simulated wave functions as a function of time for different values of  $Q$  in the  $s$ -NQS. The infidelity is defined as  $I(t) = 1 - |\langle \psi_{\text{exact}}(t) | \psi_{\text{NQS}}(t) \rangle|^2$  where  $|\psi_{\text{exact}}(t)\rangle$  is obtained via exact diagonalization. Given the size of the system considered, the infidelity can be evaluated exactly. A larger value of  $Q$  allows the wave function to capture finer time variations, effectively fitting more points within a given interval. This increases the expressibility of the  $s$ -NQS. However, it comes at the cost of a larger number of parameters. In Fig. 2(b), we also plot the infidelity obtained using p-tVMC [25, 36]. For the latter, we used AdamW as an optimizer for a direct comparison to our  $s$ -NQS approach. For both the p-tVMC and  $s$ -NQS approaches, we use a RBM with  $\alpha = 5$  as the base neural network. All expectation values and gradients are computed exactly, without sampling. We observe that increasing  $Q$  from 2 to 7 leads to a substantial reduction in infidelity. Interestingly, the  $s$ -NQS achieves an infidelity that is orders of magnitude lower than that of p-tVMC.

It is also important to compare the total number of parameters needed to perform these evolutions. For the p-tVMC evolution over  $K$  time steps, we require  $K$  neural networks, and consequently  $KN_p$  parameters, where  $N_p$  is the number of neural network parameters at each time. This would allow us to recompute all observables at any of the time steps  $k\Delta t$  [52]. In contrast, the  $s$ -NQS requires only  $QN_p$  parameters, and since  $Q < K$  this leads to a significant reduction in memory usage. Furthermore, the wave function can be evaluated at arbitrary time points, not limited to  $k\Delta t$ , and remains accurate even beyond the training interval.

## B. Larger system simulation

We now apply the  $s$ -NQS approach to a larger system with  $L = 30$  spins and open boundary conditions. The system parameters remain the same as in the small-system case, and we use a time step  $J\Delta t = 0.005$ , a time interval  $J\tau = 0.2$ , and a time window  $JT = 2$ . In large system simulations, smaller time steps  $\Delta t$  are often required to maintain numerical stability and accuracy.

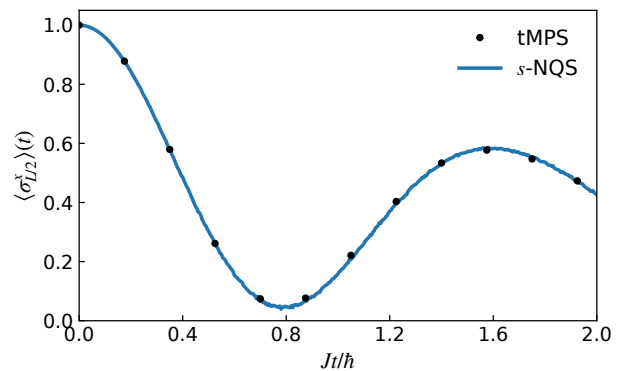


FIG. 3. Time evolution of the transverse magnetization  $\langle \sigma_{L/2}^x \rangle(t)$  after quench in 1D tilted Ising model with  $L = 30$  spins and open boundary conditions. The solid blue line represents the results from  $s$ -NQS with  $\alpha = 5$  and  $Q = 7$ , while the black dots correspond to time-dependent matrix product states (tMPS) simulations. The parameters are  $J\Delta t/\hbar = 0.005$ ,  $J\tau/\hbar = 0.2$ , and  $JT/\hbar = 2$ .

However, this increases the number of training points per interval and thus the optimization overhead. Here, we adopt a coarse-to-fine strategy where parameters optimized at larger time steps serve as initialization for finer resolutions. This is possible thanks to the parameterization of the  $s$ -NQS, whose time-independent parameters  $\{\theta_{j,q}\}$  allow for accurate predictions at untrained intermediate times.

The time evolution of  $\langle \sigma_{L/2}^x \rangle$  is shown in Fig. 3. The results obtained from  $s$ -NQS (solid blue line) with  $\alpha = 5$  and  $Q = 7$  are shown in comparison with those from time-dependent matrix product states tMPS [13, 14] (black dots) simulations. The agreement demonstrates the accuracy of the method at relatively long times and highlights the expressivity of the  $s$ -NQS ansatz when applied to large-scale, nonintegrable many-body systems.

## V. CONCLUSIONS

In this work, we have introduced a smoothly parameterized neural quantum state ( $s$ -NQS) ansatz, in which the variational parameters are defined as linear combinations of temporal basis functions with time-independent variational parameters. Our approach achieves accurate simulations of the dynamics of a non-integrable many-body system using fewer cumulative parameters than step-by-step variational methods. Moreover, the smooth parameterization provides reliable initialization across intervals, leading to enhanced stability and efficiency in training. These features make the  $s$ -NQS a scalable and effective framework for modeling complex quantum dynamics.

To further enhance the effectiveness of the  $s$ -NQS approach, future directions include using alternative, and/or higher-order, approximations of the evolution op-

erator, as proposed in Ref. [26], and achieving this ansatz with more expressive network architectures such as convolutional neural networks or transformers. Another promising direction involves exploring alternative temporal basis functions beyond the Chebyshev polynomials used in this work. Fourier modes, for instance, as employed in Ref. [28], may offer advantages in capturing long-time behavior and periodic features of the system. Furthermore, while we employed the AdamW optimizer throughout this study, alternative optimization schemes, such as stochastic reconfiguration, may provide improved convergence properties and should be considered in future work. A thorough comparison with state-of-the-art neural quantum states methods as described in [26–28], and potential integration with them, would also be an interesting research direction.

An important underlying assumption of the  $s$ -NQS ansatz is the continuity of the quantum evolution. A natural question we will tackle in future works is whether  $s$ -NQS can effectively capture dynamics in systems undergoing dynamical phase transitions [10], where certain quantities manifest a discontinuous behavior. We emphasize that true phase transitions occur only in the thermodynamic limit, making it essential to understand how the

expressivity of the ansatz, especially the number and type of temporal basis functions, scales with system size. Beyond unitary time evolution, the  $s$ -NQS approach could also be extended to non-unitary dynamics in open quantum systems, imaginary-time evolution for ground-state searches, and the study of classical systems.

## ACKNOWLEDGMENTS

We are grateful to A. Burger, E. Chong, A. Sinibaldi and L. Wang for fruitful discussions. D.P. acknowledges support from the Ministry of Education Singapore, under the grant MOE-T2EP50123-0046, D.W. acknowledges support from the National Research Foundation, Singapore and the Agency for Science, Technology and Research (A\*STAR) under the Quantum Engineering Programme (NRF2021-QEP2-02-P03) and from CQT Core Funding Grant CQT.SUTD.2025.01. W.Z acknowledges support from CQT Core Funding Grant A-0009609-38-00.

The computational work for this article was partially performed at the National Supercomputing Centre, Singapore [53], and on cloud resources provided by NVIDIA Academic Grant Program.

- 
- [1] L. D’Alessio, Y. Kafri, A. Polkovnikov, and M. Rigol, From quantum chaos and eigenstate thermalization to statistical mechanics and thermodynamics, *Adv. Phys.* **65**, 239 (2016).
  - [2] M. Moeckel and S. Kehrein, Interaction Quench in the Hubbard Model, *Phys. Rev. Lett.* **100**, 175702 (2008).
  - [3] M. Gring, M. Kuhnert, T. Langen, T. Kitagawa, B. Rauer, M. Schreitl, I. Mazets, D. A. Smith, E. Demler, and J. Schmiedmayer, Relaxation and Prethermalization in an Isolated Quantum System, *Science* **337**, 1318 (2012).
  - [4] T. Mori, T. N. Ikeda, E. Kaminishi, and M. Ueda, Thermalization and prethermalization in isolated quantum systems: A theoretical overview, *J. Phys. B: At. Mol. Opt. Phys.* **51**, 112001 (2018).
  - [5] P. Reimann and L. Dabelow, Typicality of Prethermalization, *Phys. Rev. Lett.* **122**, 080603 (2019).
  - [6] K. Mallayya and M. Rigol, Prethermalization, thermalization, and Fermi’s golden rule in quantum many-body systems, *Phys. Rev. B* **104**, 184302 (2021).
  - [7] D. Basko, I. Aleiner, and B. Altshuler, Metal–insulator transition in a weakly interacting many-electron system with localized single-particle states, *Annals of Physics* **321**, 1126 (2006).
  - [8] D. A. Abanin, E. Altman, I. Bloch, and M. Serbyn, Colloquium: Many-body localization, thermalization, and entanglement, *Reviews of Modern Physics* **91**, 021001 (2019).
  - [9] M. Heyl, A. Polkovnikov, and S. Kehrein, Dynamical quantum phase transitions in the transverse-field Ising model, *Phys. Rev. Lett.* **110**, 135704 (2013).
  - [10] M. Heyl, Dynamical quantum phase transitions: a review, *Reports on Progress in Physics* **81**, 054001 (2018).
  - [11] C. J. Turner, A. A. Michailidis, D. A. Abanin, M. Serbyn, and Z. Papić, Weak ergodicity breaking from quantum many-body scars, *Nature Physics* **14**, 745 (2018).
  - [12] L. Capizzi, J. Wang, X. Xu, L. Mazza, and D. Poletti, Hydrodynamics and the eigenstate thermalization hypothesis, *Phys. Rev. X* **15**, 011059 (2025).
  - [13] F. Verstraete, V. Murg, and J. I. Cirac, Matrix product states, projected entangled pair states, and variational renormalization group methods for quantum spin systems, *Advances in physics* **57**, 143 (2008).
  - [14] U. Schollwöck, The density-matrix renormalization group in the age of matrix product states, *Annals of Physics* **326**, 96 (2011), January 2011 Special Issue.
  - [15] R. Orús, A practical introduction to tensor networks: Matrix product states and projected entangled pair states, *Annals of physics* **349**, 117 (2014).
  - [16] D.-L. Deng, X. Li, and S. Das Sarma, Quantum entanglement in neural network states, *Phys. Rev. X* **7**, 021021 (2017).
  - [17] G. Carleo, I. Cirac, K. Cranmer, L. Daudet, M. Schuld, N. Tishby, L. Vogt-Maranto, and L. Zdeborová, Machine learning and the physical sciences, *Rev. Mod. Phys.* **91**, 045002 (2019).
  - [18] H. Lange, A. Van de Walle, A. Abedinnia, and A. Bohrdt, From architectures to applications: a review of neural quantum states, *Quantum Science and Technology* **9**, 040501 (2024).
  - [19] M. Schmitt and M. Heyl, Quantum many-body dynamics in two dimensions with artificial neural networks, *Phys. Rev. Lett.* **125**, 100503 (2020).
  - [20] I. L. Gutiérrez and C. B. Mendl, Real time evolution with

- neural-network quantum states, *Quantum* **6**, 627 (2022).
- [21] A. Sinibaldi, C. Giuliani, G. Carleo, and F. Vicentini, Unbiasing time-dependent variational monte carlo by projected quantum evolution, *Quantum* **7**, 1131 (2023).
- [22] K. Donatella, Z. Denis, A. Le Boité, and C. Ciuti, Dynamics with autoregressive neural quantum states: Application to critical quench dynamics, *Phys. Rev. A* **108**, 022210 (2023).
- [23] H. Bureau and M. Heyl, Unitary long-time evolution with quantum renormalization groups and artificial neural networks, *Phys. Rev. Lett.* **127**, 050601 (2021).
- [24] M. Schmitt, M. M. Rams, J. Dziarmaga, M. Heyl, and W. H. Zurek, Quantum phase transition dynamics in the two-dimensional transverse-field ising model, *Science Advances* **8**, eabl6850 (2022).
- [25] W. Zhang, B. Xing, X. Xu, and D. Poletti, *Paths towards time evolution with larger neural-network quantum states* (2024), [arXiv:2406.03381 \[quant-ph\]](https://arxiv.org/abs/2406.03381).
- [26] L. Gravina, V. Savona, and F. Vicentini, *Neural projected quantum dynamics: a systematic study* (2024), [arXiv:2410.10720 \[quant-ph\]](https://arxiv.org/abs/2410.10720).
- [27] A. V. de Walle, M. Schmitt, and A. Bohrdt, *Many-body dynamics with explicitly time-dependent neural quantum states* (2024), [arXiv:2412.11830 \[quant-ph\]](https://arxiv.org/abs/2412.11830).
- [28] A. Sinibaldi, D. Hendry, F. Vicentini, and G. Carleo, *Time-dependent neural galerkin method for quantum dynamics* (2024), [arXiv:2412.11778 \[quant-ph\]](https://arxiv.org/abs/2412.11778).
- [29] A. Chen, V. D. Naik, and M. Heyl, *Convolutional transformer wave functions* (2025), [arXiv:2503.10462 \[cond-mat.dis-nn\]](https://arxiv.org/abs/2503.10462).
- [30] F. Vicentini, A. Biella, N. Regnault, and C. Ciuti, Variational neural-network ansatz for steady states in open quantum systems, *Phys. Rev. Lett.* **122**, 250503 (2019).
- [31] A. Nagy and V. Savona, Variational quantum monte carlo method with a neural-network ansatz for open quantum systems, *Phys. Rev. Lett.* **122**, 250501 (2019).
- [32] N. Yoshioka and R. Hamazaki, Constructing neural stationary states for open quantum many-body systems, *Phys. Rev. B* **99**, 214306 (2019).
- [33] M. J. Hartmann and G. Carleo, Neural-network approach to dissipative quantum many-body dynamics, *Phys. Rev. Lett.* **122**, 250502 (2019).
- [34] M. Reh, M. Schmitt, and M. Gärttner, Time-dependent variational principle for open quantum systems with artificial neural networks, *Phys. Rev. Lett.* **127**, 230501 (2021).
- [35] G. Carleo and M. Troyer, Solving the quantum many-body problem with artificial neural networks, *Science* **355**, 602 (2017).
- [36] A. Sinibaldi, C. Giuliani, G. Carleo, and F. Vicentini, Unbiasing time-dependent Variational Monte Carlo by projected quantum evolution, *Quantum* **7**, 1131 (2023).
- [37] M. Schmitt and M. Heyl, *Simulating dynamics of correlated matter with neural quantum states* (2025), [arXiv:2506.03124 \[quant-ph\]](https://arxiv.org/abs/2506.03124).
- [38] S. Sorella, Green function monte carlo with stochastic reconfiguration, *Phys. Rev. Lett.* **80**, 4558 (1998).
- [39] S. Sorella, M. Casula, and D. Rocca, Weak binding between two aromatic rings: Feeling the van der waals attraction by quantum monte carlo methods, *The Journal of chemical physics* **127** (2007).
- [40] C. Kollath, A. M. Läuchli, and E. Altman, Quench dynamics and nonequilibrium phase diagram of the bose-hubbard model, *Phys. Rev. Lett.* **98**, 180601 (2007).
- [41] A. Polkovnikov, K. Sengupta, A. Silva, and M. Vengalattore, Colloquium: Nonequilibrium dynamics of closed interacting quantum systems, *Rev. Mod. Phys.* **83**, 863 (2011).
- [42] V. I. Yukalov, Equilibration and thermalization in finite quantum systems, *Laser Physics Letters* **8**, 485 (2011).
- [43] A. C. Cassidy, C. W. Clark, and M. Rigol, Generalized thermalization in an integrable lattice system, *Phys. Rev. Lett.* **106**, 140405 (2011).
- [44] E. Canovi, D. Rossini, R. Fazio, G. E. Santoro, and A. Silva, Quantum quenches, thermalization, and many-body localization, *Phys. Rev. B* **83**, 094431 (2011).
- [45] M. Rigol, Quantum quenches and thermalization in one-dimensional fermionic systems, *Phys. Rev. A* **80**, 053607 (2009).
- [46] I. Loshchilov and F. Hutter, Decoupled weight decay regularization, in *International Conference on Learning Representations* (2019).
- [47] D. W. Berry, G. Ahokas, R. Cleve, and B. C. Sanders, Efficient Quantum Algorithms for Simulating Sparse Hamiltonians, *Communications in Mathematical Physics* **270**, 359 (2007).
- [48] N. Hatano and M. Suzuki, Finding Exponential Product Formulas of Higher Orders, in *Lecture Notes in Physics, Berlin Springer Verlag*, Vol. 679, edited by A. Das and B. K. Chakrabarti (2005) p. 37.
- [49] J. M. Deutsch, Quantum statistical mechanics in a closed system, *Phys. Rev. A* **43**, 2046 (1991).
- [50] M. Srednicki, Chaos and quantum thermalization, *Phys. Rev. E* **50**, 888 (1994).
- [51] L. D'Alessio, Y. Kafri, A. Polkovnikov, and M. Rigol, From quantum chaos and eigenstate thermalization to statistical mechanics and thermodynamics, *Advances in Physics* **65**, 239 (2016).
- [52] In case one would choose a limited set of observable a priori, and does not wish to be able to recompute the evolution over certain time steps, one can keep only  $2N_p$  parameters.
- [53] <https://www.nscg.sg/>.



## APPENDIX: SUPPLEMENTARY MATERIAL

### Appendix A: Connecting two consecutive time windows

The first few Chebyshev polynomials and their first few derivatives are given by

$$\begin{array}{ccccccc} T_1(t) = 1, & T_1(t)' = 0, & T_1(t)'' = 0 & T_1(t)''' = 0 & \dots \\ T_2(t) = t, & T_2(t)' = 1, & T_2(t)'' = 0 & T_2(t)''' = 0 & \dots \\ T_3(t) = 2t^2 - 1, & T_3(t)' = 4t, & T_3(t)'' = 4 & T_3(t)''' = 0 & \dots \\ T_4(t) = 4t^3 - 3t, & T_4(t)' = 12t^2 - 3, & T_4(t)'' = 24t & T_4(t)''' = 24 & \dots \\ \dots & \dots & \dots & \dots & \dots \end{array}$$

In our study, we consider the scaling-shifting functions  $r_i(t)$  as simply a linear shift function with no scaling. To lighten the notation, in this section we will use  $\theta_{j,q}^{[(k-1)T, kT]} \equiv \theta_{j,q}$  and  $\theta_{j,q}^{[kT, (k+1)T]} \equiv \Theta_{j,q}$ . We can thus write

$$\sum_{q=0}^{Q-1} \theta_{j,q} \frac{d^n T_q(t)}{dt^n} \Big|_{t=1} = \sum_{q'=0}^{Q-1} \Theta_{j,q'} \frac{d^n T_q(t)}{dt^n} \Big|_{t=-1}. \quad (\text{A1})$$

For clarity, we here introduce an example. Taking  $Q = 3$ , we can connect the windows from the second derivative

$$\begin{aligned} T_3(1)''\theta_{j,3} &= T_3(-1)''\Theta_{j,3} \\ \theta_{j,3} &= \Theta_{j,3} \end{aligned}$$

and then, obtained  $\Theta_{j,3}$ , we can, using the equations with the first time derivative, compute  $\Theta_{j,2}$

$$\begin{aligned} T_2(1)'\theta_{j,2} + T_3(1)'\theta_{j,3} &= T_2(-1)'\Theta_{j,2} + T_3(-1)'\Theta_{j,3} \\ \theta_{j,2} + 4\theta_{j,3} &= \Theta_{j,2} - 4\Theta_{j,3} \\ \Theta_{j,2} &= \theta_{j,2} + 8\theta_{j,3}, \end{aligned}$$

and we can thus compute  $\Theta_{j,1}$  from

$$\begin{aligned} T_1(1)\theta_{j,1} + T_2(1)\theta_{j,2} + T_3(1)\theta_{j,3} &= T_1(-1)\Theta_{j,1} + T_2(-1)\Theta_{j,2} + T_3(-1)\Theta_{j,3} \\ \theta_{j,1} + \theta_{j,2} + \theta_{j,3} &= \Theta_{j,1} - \Theta_{j,2} + \Theta_{j,3} \\ \Theta_{j,1} &= \theta_{j,1} + \theta_{j,2} + \theta_{j,3} + \theta_{j,2} + 8\theta_{j,3} - \theta_{j,3} \\ \Theta_{j,1} &= \theta_{j,1} + 2\theta_{j,2} + 8\theta_{j,3}. \end{aligned}$$

### Appendix B: Taylor Expansion

Here, we give more details on how to use the Taylor expansion to compute the overlap  $C_k$  at time point  $k\Delta t$ . The unitary operator is  $U(\Delta t) = e^{-iH\Delta t}$ , which can be approximated by Taylor expansion up to the second order

$$\hat{U}(\Delta t) = e^{-i\hat{H}\Delta t} \approx \hat{\mathbb{I}} - i\hat{H}\Delta t - \frac{1}{2}(\Delta t\hat{H})^2 \equiv \hat{U}_{\text{Taylor}} \quad (\text{B1})$$

where  $\hat{\mathbb{I}}$  is the identity operator. Given an overlap  $C_k$  at the time point  $k\Delta t$  and  $k \neq 0$ , the overlap can be written as

$$\begin{aligned} C_k &= \frac{\langle \psi_{\vartheta(k\Delta t)} | \hat{U}_{\text{Taylor}} | \psi_{\vartheta((k-1)\Delta t)} \rangle}{\langle \psi_{\vartheta(k\Delta t)} | \psi_{\vartheta(k\Delta t)} \rangle} \cdot \frac{\langle \psi_{\vartheta((k-1)\Delta t)} | \hat{U}_{\text{Taylor}}^\dagger | \psi_{\vartheta(k\Delta t)} \rangle}{\langle \psi_{\vartheta((k-1)\Delta t)} | \psi_{\vartheta((k-1)\Delta t)} \rangle} \\ &= C_{k-1,k}(\hat{U}_{\text{Taylor}}) \cdot C_{k,k-1}(\hat{U}_{\text{Taylor}}^\dagger) \end{aligned} \quad (\text{B2})$$

For the term  $C_{k-1,k}(\hat{U}_{\text{Taylor}})$ , we have

$$\begin{aligned} C_{k-1,k}(U_{\text{Taylor}}) &= \frac{\langle \psi_{\vartheta(k\Delta t)} | \hat{\mathbb{I}} - i\hat{H}\Delta t - \frac{1}{2}(\hat{H}\Delta t)^2 | \psi_{\vartheta((k-1)\Delta t)} \rangle}{\langle \psi_{\vartheta(k\Delta t)} | \psi_{\vartheta(k\Delta t)} \rangle} \\ &= \frac{\langle \psi_{\vartheta(k\Delta t)} | \hat{\mathbb{I}} | \psi_{\vartheta((k-1)\Delta t)} \rangle}{\langle \psi_{\vartheta(k\Delta t)} | \psi_{\vartheta(k\Delta t)} \rangle} - i\Delta t \frac{\langle \psi_{\vartheta(k\Delta t)} | \hat{H} | \psi_{\vartheta((k-1)\Delta t)} \rangle}{\langle \psi_{\vartheta(k\Delta t)} | \psi_{\vartheta(k\Delta t)} \rangle} - \frac{1}{2}(\Delta t)^2 \frac{\langle \psi_{\vartheta(k\Delta t)} | \hat{H}\hat{H} | \psi_{\vartheta((k-1)\Delta t)} \rangle}{\langle \psi_{\vartheta(k\Delta t)} | \psi_{\vartheta(k\Delta t)} \rangle} \end{aligned} \quad (\text{B3})$$

We can rewrite the first term of Eq. (B3) as

$$\begin{aligned}
\frac{\langle \psi_{\vartheta(k\Delta t)} | \hat{\mathbb{I}} | \psi_{\vartheta((k-1)\Delta t)} \rangle}{\langle \psi_{\vartheta(k\Delta t)} | \psi_{\vartheta(k\Delta t)} \rangle} &= \frac{\sum_{\mathbf{x}} \psi_{k\Delta t}^*(\mathbf{x}) \sum_{\mathbf{x}'} \mathbb{I}_{\mathbf{x}\mathbf{x}'} \psi_{(k-1)\Delta t}(\mathbf{x}')}{\sum_{\boldsymbol{\omega}} |\psi_{k\Delta t}(\boldsymbol{\omega})|^2} \\
&= \sum_{\mathbf{x}} \frac{|\psi_{k\Delta t}(\mathbf{x})|^2}{\sum_{\boldsymbol{\omega}} |\psi_{k\Delta t}(\boldsymbol{\omega})|^2} \sum_{\mathbf{x}'} \mathbb{I}_{\mathbf{x}\mathbf{x}'} \frac{\psi_{(k-1)\Delta t}(\mathbf{x}')}{\psi_{k\Delta t}(\mathbf{x})} \\
&= \sum_{\mathbf{x}} P_{k\Delta t}(\mathbf{x}) \frac{\psi_{(k-1)\Delta t}(\mathbf{x})}{\psi_{k\Delta t}(\mathbf{x})},
\end{aligned} \tag{B4}$$

the second term as

$$\begin{aligned}
\frac{\langle \psi_{\vartheta(k\Delta t)} | \hat{H} | \psi_{\vartheta((k-1)\Delta t)} \rangle}{\langle \psi_{\vartheta(k\Delta t)} | \psi_{\vartheta(k\Delta t)} \rangle} &= \frac{\sum_{\mathbf{x}} \psi_{k\Delta t}^*(\mathbf{x}) \sum_{\mathbf{x}'} H_{\mathbf{x}\mathbf{x}'} \psi_{(k-1)\Delta t}(\mathbf{x}')}{\sum_{\boldsymbol{\omega}} |\psi_{k\Delta t}(\boldsymbol{\omega})|^2} \\
&= \sum_{\mathbf{x}} \frac{|\psi_{k\Delta t}(\mathbf{x})|^2}{\sum_{\boldsymbol{\omega}} |\psi_{k\Delta t}(\boldsymbol{\omega})|^2} \sum_{\mathbf{x}'} H_{\mathbf{x}\mathbf{x}'} \frac{\psi_{(k-1)\Delta t}(\mathbf{x}')}{\psi_{k\Delta t}(\mathbf{x})} \\
&= \sum_{\mathbf{x}} P_{k\Delta t}(\mathbf{x}) E_{\text{loc}}(\mathbf{x}),
\end{aligned} \tag{B5}$$

and the third term as

$$\begin{aligned}
\frac{\langle \psi_{\vartheta(k\Delta t)} | \hat{H} \hat{H} | \psi_{\vartheta((k-1)\Delta t)} \rangle}{\langle \psi_{\vartheta(k\Delta t)} | \psi_{\vartheta(k\Delta t)} \rangle} &= \frac{\langle \psi_{\vartheta(k\Delta t)} | \hat{H} \sum_{\mathbf{y}} |\mathbf{y}\rangle \langle \mathbf{y}| \hat{H} | \psi_{\vartheta((k-1)\Delta t)} \rangle}{\langle \psi_{\vartheta(k\Delta t)} | \psi_{\vartheta(k\Delta t)} \rangle} \\
&= \frac{\sum_{\mathbf{x}} \psi_{k\Delta t}^*(\mathbf{x}) \sum_{\mathbf{y}} H_{\mathbf{x}\mathbf{y}} \sum_{\mathbf{x}'} H_{\mathbf{y}\mathbf{x}'} \psi_{(k-1)\Delta t}(\mathbf{x}')}{\sum_{\boldsymbol{\omega}} |\psi_{k\Delta t}(\boldsymbol{\omega})|^2} \\
&= \sum_{\mathbf{x}} \frac{|\psi_{k\Delta t}(\mathbf{x})|^2}{\sum_{\boldsymbol{\omega}} |\psi_{k\Delta t}(\boldsymbol{\omega})|^2} \sum_{\mathbf{y}} H_{\mathbf{x}\mathbf{y}} \sum_{\mathbf{x}'} H_{\mathbf{y}\mathbf{x}'} \frac{\psi_{(k-1)\Delta t}(\mathbf{x}')}{\psi_{k\Delta t}(\mathbf{x})} \\
&= \sum_{\mathbf{x}} P_{k\Delta t}(\mathbf{x}) \sum_{\mathbf{y}} H_{\mathbf{x}\mathbf{y}} \sum_{\mathbf{x}'} H_{\mathbf{y}\mathbf{x}'} \frac{\psi_{(k-1)\Delta t}(\mathbf{x}')}{\psi_{k\Delta t}(\mathbf{x})}.
\end{aligned} \tag{B6}$$